Volumetric diffusers: Pseudorandom cylinder arrays on a periodic lattice, Hughes, RJ; Angus, JAS; Cox, TJ, et al., Journal of the acoustical society of america **128(**5) 2847-2856 Published: Nov 2010, DOI 10.1121/1.3493455

Volumetric diffusers: pseudorandom cylinder arrays on a periodic lattice

Richard J. Hughes[1, a)]

Jamie A. S. Angus[1]

Trevor J. Cox[1]

Gillian G. Gehring[2]

Mark Pogson[2]

Olga Umnova[1]

David M. Whittaker[2]

[1]Acoustics Research Centre, University of Salford, Salford, Greater Manchester, M5 4WT, United Kingdom

[2]Department of Physics and Astronomy, The University of Sheffield, Sheffield, S3 7RH, United Kingdom

Date manuscript uploaded: 11/06/2010

Suggested Running Title: periodic cylinder volume diffuser

[a)] Electronic mail: r.j.hughes@pgr.salford.ac.uk

Volumetric diffusers: Pseudorandom cylinder arrays on a periodic lattice, Hughes, RJ; Angus, JAS; Cox, TJ, et al., Journal of the acoustical society of america **128(**5) 2847-2856 Published: Nov 2010, DOI 10.1121/1.3493455

ABSTRACT

Most conventional diffusers take the form of a surface based treatment, and as a result can only operate in hemispherical space. Placing a diffuser in the volume of a room might provide greater efficiency by allowing scattering into the whole space. A periodic cylinder array (or sonic crystal) produces periodicity lobes and uneven scattering. Introducing defects into an array, by removing or varying the size of some of the cylinders, can enhance their diffusing abilities. This paper applies number theoretic concepts to create cylinder arrays that have more even scattering. Predictions using a Boundary Element Method are compared to measurements to verify the model, and suitable metrics are adopted to evaluate performance. Arrangements with good aperiodic autocorrelation properties tend to produce the best results. At low frequency power is controlled by object size and at high frequency diffusion is dominated by lattice spacing and structural similarity. Consequently the operational bandwidth is rather small. By using sparse arrays and varying cylinder sizes, a wider bandwidth can be achieved.

PACS numbers: 43.55.Br, 43.20.El, 43.20.Fn, 43.55.-n.

Volumetric diffusers: Pseudorandom cylinder arrays on a periodic lattice, Hughes, RJ; Angus, JAS; Cox, TJ, et al., Journal of the acoustical society of america **128(**5) 2847-2856 Published: Nov 2010, DOI 10.1121/1.3493455

I. INTRODUCTION

Diffusers can reduce unwanted artifacts such as strong echoes and coloration by breaking up reflections without removing excess energy[1]. In the 1970s, Schroeder introduced the concept of using Maximum Length Sequences (MLS) in the design of diffusers to improve sound diffusion in concert halls and reverberation chambers[2]. Since then a variety of number theoretic concepts have been developed[3-5]. Most conventional diffusers are put on the surfaces of rooms, and as a result can only operate in (2π) hemispherical space. In addition their low frequency performance is often restricted by available depth. By considering a structure placed in the volume of the room, it becomes possible to operate on 4π space, with sound being received from and scattered into all possible directions[6]. This provides a possible increase in efficiency[7] and is a solution adopted in many reverberation chambers. Furthermore by providing many reflection paths a volume device may promote multiple scattering, spreading energy temporally as well as spatially, and potentially bypassing the low frequency limitation. A constraint on these structures is that they cannot be placed where they interfere with a room's functionality, for example in the line-of-sight of an audience. It may be possible however, to find a number of suitable locations for their application, depending on the use of the space.

Volumetric diffusers, whether by accident or design, are not an entirely new topic; a chandelier may be considered to be a volume diffuser, whilst large curved panels suspended in reverberation chambers[8] and overhead stage-canopies[9] provide examples of purpose built structures. These designs are application specific, and would make unsuitable ready-to-install units intended for a variety of room types. There is therefore a need for an appropriate methodology for their design, measurement and analysis.

Recent investigations into the use of slats[10] demonstrated a volumetric equivalent to the Binary Amplitude Diffuser (BAD)[5], whereby transmission is analogous to absorption. Uni-polar binary sequences determined the arrangement of the slats, with a value of 1 or 0 representing the inclusion or omittance of each element respectively. This was shown first for a single layer, before depth was added through multiple layers allowing cancellation of the back-scattered specular lobe. Arrangements however were heavily dependent on line-of-sight through the array, with insufficient energy penetrating into the structure. Cox *et al.*[11] extended the concept to a percolation structure allowing both vertical and horizontal slats to promote energy channeling. Preliminary results indicated that improvements could be made.

In this study a new kind of volumetric diffuser is considered, and builds upon previous results presented by the authors[12]. Considering arrangements akin to a sonic crystal[13,14], periodic arrays of cylinders are investigated. Previous work in this area has predominantly focused on attenuation by arrays at specific frequencies, known as band-gaps, rather than on the spatial distribution of its scattered field. A typical sonic crystal will spread energy temporally, but produces inherent grating lobes and therefore makes a poor diffuser whose behavior varies significantly with position and frequency. In this study, the arrays have relatively low occupancy as shown in Figure 1, which makes the periodicity effects less dominant. The reasons for keeping an underlying periodicity are that it could make manufacture easier and allows the application of number theoretic concepts.

At first single layer diffusers are considered, before multilayer square lattice structures are explored. Later alternative lattice shapes are considered as well as the effect of varying individual cylinder size. A simple Fourier approximation is used to inform potentially suitable sequences, whilst a Boundary Element Method (BEM) based on the Helmholtz-Kirchhoff

integral equation is used to gain more accurate predictions[15], and this is verified through selective measurements. All predictions are performed in 2D considering scattering in one plane only and assume rigid surfaces to ensure maximum preservation of energy.

II. DEFINING APPROPRIATE METRICS

To assess a volume diffuser's effectiveness it is necessary to expand on current criteria for more conventional devices[16]. Consider the setup shown in Figure 2 where a volume diffuser is subject to a sound from a source. Unlike scattering from surface diffusers where a hemispherical area is considered, the whole field must be taken into account, which for the 2D case here means a full circle of receiver locations, rather than the conventional semicircular arc. Both source and receivers are assumed to be in the far-field[16] of the diffusing structure of width *D*, centered on the origin. Unless otherwise stated, normal incidence ($\theta = 0^{\circ}$) is assumed.

A. Scattering Uniformity

The standard diffusion coefficient[16], δ_θ, is used to assess scattering uniformity, given as:

$$\delta_\theta = \frac{\left(\sum_{n=1}^{N}\left|p_{s,n}\right|\right)^2 - \sum_{n=1}^{N}\left|p_{s,n}\right|^2}{(N-1)\sum_{n=1}^{N}\left|p_{s,n}\right|^2} \tag{1}$$

Where $p_{s,n}$ represents the pressure scattered from the diffuser at the *n*-th receiver over the evaluated region. Each receiver though observes the total sound field - a summation of both the incident sound direct from the source, and a scattered sound due to the presence of the diffuser. The back-scattered zone (BSZ, $\theta - 90^{\circ} \leq \theta_r \leq \theta + 90^{\circ}$) can be straightforwardly treated, as the scattered component is sufficiently separated in time from the incident sound to be considered separately. This is the way in which many conventional surface diffusers are analyzed.

The remaining forward-scattered zone (FSZ, $\theta + 90^{\circ} < \theta_r < \theta + 270^{\circ}$) is more complex. In the geometric shadow zone (GSZ) behind the diffuser, where direct line of sight between source and receivers may be blocked, the incident and scattered sound will arrive at comparable times and their interference cannot be ignored. Here therefore the scattered pressure alone becomes meaningless, and it is the attenuation properties of the array which are more of concern. Between the back-scattered and shadow zone, there is a region of ambiguity where it becomes unclear whether the total or scattered pressure should be used. In reality however, a receiver located close to the shadow zone implies a diffuser installed near to an observers line of sight of an acoustic source, which in spaces such as auditoria for example – where the audience requires an unobstructed view of a stage – should be avoided. Sound scattered into these angles however will continue to propagate and contribute towards a diffuse field, and so uniformity is still desirable. A diffusion coefficient for volume diffusers is therefore proposed, considering all receiver angles excluding the shadow zone. This region is referred to as the geometric visible zone (GVZ), and hence this coefficient is given as $\delta_{\theta,GVZ}$.

B. Scattered Power

A diffuser whose elements are much smaller than wavelength can generate uniform scattering, however, it actually causes little perturbance to the sound field and is effectively almost acoustically transparent. For this reason the scattered power also needs considering. This is done via a scattered intensity ratio, $L_{IR,\theta,BSZ}$. This compares the back-scattered energy to that of a reference structure whose scattering properties are well understood – in this case a flat plate of equal width, D, to the diffuser - whilst normalizing to account for differences in model setup. The ratio is defined as:

$$L_{IR,\theta,BSZ} = 10\log_{10}\left(\frac{\sum_{n=1}^{N}\left|p_{diff,n}\right|^2}{\sum_{n=1}^{N}\left|p_{ref,n}\right|^2}\right) \quad (2)$$

Where $p_{diff,n}$ and $p_{ref,n}$ are the scattered pressures at the n-th receiver in the back-scattered zone for the diffuser and reference structure respectively.

A value of -3dB relative to the reference plate forms a suitable design target for a volume array. This means that half the incident energy is back-scattered. The choice of -3dB was somewhat arbitrary, and it would be possible to design for other target values.

III. CONVENTIONAL DIFFUSER DESIGN THEORY

A. The Fourier approximation

Consider the arrangement shown in Figure 3, depicting an $M\times N$ rectangular grid of point scattering elements, with element spacing of d_x and d_y in the x and y directions respectively. This represents the generalized 2D case. The structure is subject to an incident plane wave p_i of wavelength λ, arriving from angle θ. The scattered pressure, p_s, is evaluated for a circle of receivers with location determined by angle, θ_r. Far-field conditions are assumed. If all elements are assumed to have the same individual pressure polar response for all angles of incidence and reflection, $e(\theta, \theta_r)$, with individual reflection coefficients independent of angle, R_n, then for a given receiver the following holds.

$$p_s(\theta,\theta_r) = e(\theta,\theta_r)\sum_{n=0}^{N-1} R_n e^{j2\pi n d_y(\sin\theta+\sin\theta_r)/\lambda} \quad (3)$$

Where only first order reflections are considered for simplicity in this model. This follows from the well known theory in optics that the diffraction pattern of a periodic structure is equal to the product of the diffraction pattern of the base element and that of the array[17]. Eq. 3

represents a Discrete Fourier Transform (DFT), where $p_s(\theta, \theta_r)$ is the angle dependent scattered pressure in the $d_y(sin\theta+sin\theta_r)/\lambda$ domain. A set of coefficients whose DFT is maximally flat is therefore desired. Wiener-Khinchin theorem states that the power spectrum of a sequence is equal to the Fourier Transform of its Autocorrelation Function (ACF). A series of reflection coefficients whose ACF is most like a Kronecker delta function is hence desirable. A flat Fourier spectrum equates to scattering equal energy into the grating lobes, and this is what Schroeder described as 'optimal' diffusion[3]. This is not the same as even scattering into all angles.

IV. A SINGLE-LAYERED DIFFUSER

A periodic line array of scattering elements is considered first. Ideally these would both scatter energy evenly into all receiver angles and promote multiple scattering to increase reflection density in the impulse response by breaking up the scattered field in time. This structure may be arranged according to a positive binary sequence. Similar arrays have been considered previously for surface diffusers, though using semicylinders[6].

Consider a volume equivalent to the BAD panel shown in Figure 4a, comprising a series of reflecting and absorbing strips. A literal translation would be an array of both reflecting and absorbing cylinders for sequence values R_n of 1 and 0 respectively, with scattering from each element $e(\theta, \theta_r)$ given by that from a single cylinder of diameter, d_e. Absorption however is not necessary as cylinders may simply be omitted, forming the array in Figure 4b, which allows transmission rather than removal of energy. This is particularly advantageous where preservation of energy is desirable, because sound passing through the array is not lost from the room.

B. Sequences: redundancy and the Golomb ruler

It is assumed that a diffuser is not being placed alongside other identical units and consequently the Aperiodic Autocorrelation Function (AACF) is most appropriate to the work.

The Fourier approximation for the far-field polar pattern is given by the DFT of the reflection coefficients padded with zeros (effectively representing free-space), and so a sequence with a Kronecker delta like AACF is required. The AACF of a uni-polar binary sequence can be described as the number of elements separated by each unique separation distance within a sequence[18]. An even spread of separation distances is therefore sought. Repetition will result in similarity between scattering from element pairs, leading to lobing and thus uneven scattering[19]. Conversely, an even spread of separation distances should avoid emphasis.

In radar and sonar the AACF is often expressed in terms of redundancy[20]. A distance separation, or lag, is described as being redundant if it has one or more repetitions. An arrangement is described as being non-redundant if there are no redundancies, whilst a sequence with all possible distance separations with the least number of elements is said to have minimum-redundancy. One particular type of non-redundant sequences is given by the Golomb ruler[18], an example of which is shown in Figure 4, an imaginary ruler comprising a set of marks at integer positions where no two marks are the same distance apart. The total number of marks on the ruler is defined as the order, and the maximum separation distance as the length, $L = N - 1$. A Golomb ruler is said to be optimal if no shorter ruler of the same order exists, and is a special case of the non-redundant array referred to as the minimum hole array that minimizes the number of holes (missing lags) in the AACF. A sequence with no holes is said to be a perfect Golomb ruler.

C. 1D Diffusion

Figure 5a-b compares two cyclic variations of the same MLS sequence, the first being the perfect Golomb ruler shown in Figure 4b, and shows that the sequence with the more Kronecker delta like AACF produces better diffusion. At low frequency, the performance is similar to that

of the reference plate, as the structures are small relative to wavelength. With increasing frequency, and as wavelength becomes comparable to the varying cylinder separation distances, progressively more of the sidelobe energy is seen and the Golomb ruler provides a more even spread of energy. At higher frequencies, repetitions of the main specular lobe appear due to spatial aliasing, the first occurrence being at approximately 1.7kHz, and here the diffusion coefficient for both sequences begins to plateau. This agrees with previous investigations into periodic arrays of semicylinders, where at high frequency the arrangement was found to have little influence as the sidelobe behavior becomes lost within the large number of closely spaced grating lobes[6]. This is unavoidable for a 1D sequence.

V. A MULTI-LAYERED DIFFUSER

A. 2D Fourier approximation

By extending the single layered concept, a multilayer structure based on a square lattice may be envisaged. Consider the arrangement shown in Figure 3, comprising an $M \times N$ rectangular grid, where now $M \geq 1$. If all elements are again assumed to have the same individual polar response for all angles of incidence and reflection, $e(\theta, \theta_r)$, then the following holds.

$$p_s(\theta,\theta_r) = e(\theta,\theta_r)\sum_{n=0}^{N-1}\sum_{m=0}^{M-1} R_{n,m} e^{j2\pi\left[nd_y(\sin\theta+\sin\theta_r)+md_x(\cos\theta+\cos\theta_r)\right]/\lambda} \tag{4}$$

Eq. 4 is now a 2D DFT of the individual reflection coefficients $R_{n,m}$, and is again a first order scattering approximation, most valid for low fill factors and when cylinders are small relative to wavelength. This neglects multiple scattering effects, though has the benefit of allowing fast predictions. The angular variables θ and θ_r are common to both orthogonal directions, and consequently are dependent on one another, resulting in an interfering product due to periodicity in the two directions. The forward-scattered specular component interacts with

the incident field and determines attenuation in the shadow zone, whilst the sidelobe and grating lobe behavior determine the remaining scattered field. Like surface Schroeder diffusers, the addition of depth allows cancellation of the back-scattered specular lobe, giving potential for more even scattering.

B. 2D Sequence search

Again, an array is desired whose reflection coefficients, $R_{n,m}$, form a sequence whose AACF is optimal, implying a structure with an even spread of vector separations between elements. There are quite a few 2D sequences whose periodic autocorrelation properties are optimal, for example MLS, however aperiodic equivalents are less common. Furthermore unlike for periodic sequences, folding techniques such as the Chinese remainder theorem[21] cannot be applied because these assume periodicity. Consequently optimal sequences such as minimum hole arrays are often found using (intelligent) exhaustive computational searching[22], and so produce small arrays.

In order to obtain a sufficiently large sequence one alternative is to use an optimization routine, and for this a genetic algorithm and the Fourier approximation given by Eq. 4 was used. This is a simplified version of the process adopted by Romero García *et al.*[23] where targeted band gaps were created in sonic crystals, and Hakansson *et al.*[24] where focusing arrays were generated. As the Fourier approximation is based on a simple summation of (scattering) sources it is particularly suited to this type of optimization, as elements are assumed to act independently. Using this method a sequence comprising a 10×10 grid with 25% occupancy was created, and is shown in Figure 1a.

C. Measurements

Scattered pressure distributions were measured at 4:1 scale in a semi-anechoic chamber following a boundary plane procedure similar to that outlined in AES-4id-2001[16]. Figure 1b shows the setup, where the sample comprises a series of aluminum cylinders of 1m in height, arranged according to the optimized sequence of Figure 1a. These were fixed into a central sample plate that slotted into a fake floor, assumed to be acoustically rigid. The sample hole was filled with a flat board with no sample present for background measurements. An MLS signal was produced by a source located a distance of 2.5m from the array centre. Receivers were placed in a circle of radius 1.35m from the centre of the array, with an angular step of 9°.

For surface diffusers, the procedure is to separate the direct and scattered sound in the impulse responses measured at the microphones by considering time of arrival. However, behind the diffuser progressive merging of the incident and scattered field makes this impossible. As part of the procedure in AES-4id-2001, a background measurement is made without the diffuser present, and this is subtracted from the measured impulse response with the sample. While in theory this should remove the incident sound, in reality slight changes in ambient temperature can cause sound speed differences, leading to a shift in arrival time[25]. Substantial artifacts of the incident field can remain, particularly with increasing frequency and when scattering is comparatively weak.

In order to address this, a solution similar to that proposed by Robinson *et al.*[26] was adopted. Each sample and background measurement were oversampled (to give a finer resolution in time of flight) and cross-correlated, and an effective average sample drift per meter was calculated. An appropriate shift was then applied to each sample measurement signal based on their distance from the source, before downsampling back to the original sample rate. Figures 6a-

b compare the measured and BEM polar plot results for the 10×10 array at 1050Hz and 1600Hz respectively. The scattered pressure has been normalized to the incident pressure at the back receiver ($\theta_r = \theta + 180^\circ$). Agreement is generally good even for receivers towards the shadow zone, though some errors arise due to uncertainty in receiver positioning and the sensitive nature of the structure to the sound speed used for the comparison BEM model.

D. Results

Diffusion properties

Figure 7a shows the diffusion coefficient for the optimized sequence in Figure 1a. Due to the underlying periodicity, the frequencies at which spatial aliasing occurs are dominant despite the removal of cylinders. When lobing due to periodicity in the *x* and *y* directions occur at the same angle, their product results in constructive interference concentrating reflection in one direction. These are known as Bragg peaks[27], and are analogous to the flat-plate frequencies observed in Schroeder diffusers, when the difference between reflection paths become equal to a multiple of a wavelength and all wells reradiate in phase. They are also intrinsically linked through conservation of energy to the attenuation band-gaps observed in sonic crystals. It can be shown[12] that these frequencies are given by:

$$f_{\alpha,\beta} = \frac{c\left(\frac{\alpha^2}{d_x{}^2} + \frac{\beta^2}{d_y{}^2}\right)}{2\left(\frac{\alpha\cos\theta}{d_x} + \frac{\beta\sin\theta}{d_y}\right)} \tag{5}$$

$\alpha = 0, 1, 2, \ldots \qquad \beta = 0, 1, 2, \ldots$

These frequencies for the diffuser tested are shown in Figure 7a. An example of the first Bragg frequency when the energy is redirected back towards the source is shown in Figure 6a,

compared with the more evenly distributed field of Figure 6b. Although the simplified Fourier prediction of Figure 7a results in a slightly optimistic diffusion coefficient, it accurately predicts the first significant notch as well as giving an overall indication of diffusive behavior. Low frequency performance before the first Bragg frequency is relatively poor, and this is due to the limited ability of an individual cylinder to forward-scatter energy when cylinder size is small relative to wavelength. Larger cylinders would therefore be preferred, though performance is significantly better when considering a more conventional back-scattered diffusion coefficient.

For arrays with higher occupancy, diffusion notches are broader and more defined and continue on to higher frequencies. The presence of the first notch is still obvious even for sparser arrays. The ability of the Fourier method to predict these trends is not surprising as the solution is inherently linked to the vector separations between elements via the AACF, and hence the potential reflection paths within the array. A fuller multiple scattering solution must also depend on these reflection paths (though more so for low frequency as some are not possible due to shadowing, and separations do not take into account finite cylinder size). Consequently, an array whose reflection paths are uncorrelated will tend to diffuse well whether considering a single or multiple scatter solution. Cylinders closer together however will have a greater multiple scattering influence, and hence these shorter paths will be more dominant.

Scattered power

Figure 7b shows the back-scattered intensity ratio for the optimized array from Figure 1. At low frequency, the Fourier approximation provides reasonable agreement, though tends to provide an overestimate at higher frequencies, particularly at the Bragg frequencies, as shadowing and multiple scattering effects are not accounted for. High frequency performance for this level of occupancy is determined by percentage line of sight (50%), providing an

approximate -3dB plateau, whilst at low frequency there is a roll-off in scattered power. A transitional 'knee' frequency is evident when cylinder diameter, d_e, is approximately equal to a quarter wavelength. This also tends to coincide with the first Bragg peak. Consequently at low frequency the array diffuses well in the back-scattered direction though with limited efficiency, whilst at higher frequencies sufficient power is scattered, including in the forward-scattered direction, but diffusion suffers from underlying periodicity. The operational bandwidth is therefore small, and an array which allows larger cylinders or reduces the effects of periodicity is needed.

VI. ALTERNATIVE 2D CONSTRUCTION TECHNIQUES

A. The Costas array

Like the 1D case, an array ideally should have good AACF properties, implying little or no redundancy to minimize periodicity effects. The AACF of a 2D uni-polar binary sequence may be thought of as the number of elements separated by a given vector spacing – that is not only by the same distance but also direction. 2D non-redundant sequences have no repetitions of these separation vectors and so should be ideal, providing they have a sufficient number and spread of elements for them to be useful. An example is the Costas array, defined as being a permutation matrix whose separation vectors between occupied cells are unique[28]. In other words, a square $N \times N$ grid containing N elements, with one element in each row and each column and a maximum out of phase AACF coincidence of one. Costas arrays may be thought of as a 2D semi-equivalent to the Golomb ruler, and are commonly used as frequency hop patterns for sonar or radar due to their optimum ambiguity function[28].

There are a number of methods for making Costas arrays, though particularly suited to this application is the Taylor T_4 variant to the Lempel L_2 construction[28]. This method ensures a

minimum separation distance between elements, allowing larger cylinders for increased low frequency power. For a generating prime power, q^k, where q is any prime and k is an integer, the Lempel L_2 construction forms an $N \times N$ array, $a_{i,j}$, where $N = q^k - 2$, and is defined as follows:

$$a_{i,j} = \begin{cases} 1, & u^i + v^j = 1 \\ 0, & otherwise \end{cases}, \quad 1 \le i \le N, \quad 1 \le j \le N \tag{6}$$

Where u and v are primitive roots of prime q, and the operation is carried out modulo q^k. Lempel constructions have reflective symmetry about the main diagonal. The nearest possible neighboring elements therefore lie one diagonal step apart either side of the main diagonal. A special case, of which the L_2 square array in Figure 8 (top left) is an example, is formed when $u^1 + v^2 = 1$ (and $u^2 + v^1 = 1$, though this is automatically satisfied due to symmetry) which places these two elements (highlighted by gray hatched squares) in the first two rows and columns. Removal of these elements forms a new $N = q^k - 4$ Costas array known as the Taylor T_4 variant.

With the closest element pair having been removed, this now has the property of 'non-attacking chess kings' - that is no element lies within the eight surrounding cells of another. Now it is possible to form an oversampled array where the cylinder size can be greater than grid spacing, allowing sufficient scattered power to be achieved well before the first Bragg frequency. This, for a given cylinder size, effectively pushes the first Bragg peak to a higher frequency. Figure 9a-c shows the diffusion coefficient, intensity metric, and 2D AACF for the T_4 15×15 Costas array in Figure 9d. Low frequency diffusion is improved due to the larger cylinders ability to scatter energy into the forward-scattered region, whilst at high frequency the effects of periodicity are significantly reduced due to the lack of redundancy. Even though larger cylinders are present and the line of sight is completely blocked, the resulting scattered power falls within ±1dB of the -3dB target. This is due to the sparse nature of the array, with the geometric angles

of reflection no longer tending to back-scatter sound incident upon the structure via multiple scattering.

B. Alternative Lattice Shape

Ideally an array will display isotropic behavior, meaning that performance is consistent for all angles of incidence. A potential downside of an arrangement such as that of Figure 9d is a changing appearance upon rotation, which can lead to variation in scattered power due to the change in line of sight. Introducing rotational symmetry could help. Even-fold rotational symmetry however, that is when an arrangement appears the same an even number of times for one complete rotation, implies redundancy and so is undesirable. An alternative is the hexagonal (or triangular) lattice, whose potential odd three-fold rotational symmetry permits unique vector spacings. Although examples have been considered[6], these arrays do not lend themselves as easily to surface diffuser design, both in application of number theory and in terms of construction, and consequently have received little attention. Golomb *et al.*[28] however demonstrated that a hexagonal arrangement may be formed by a simple 'shear-compression' transformation of an existing square lattice array using the transformation given by:

$$\begin{bmatrix} x_t \\ y_t \end{bmatrix} = A \begin{bmatrix} x \\ y \end{bmatrix}, \qquad A = \underbrace{\begin{bmatrix} 1 & 0 \\ 0 & \sqrt{3}/2 \end{bmatrix}}_{compression} \underbrace{\begin{bmatrix} 1 & 1/2 \\ 0 & 1 \end{bmatrix}}_{shear} = \underbrace{\begin{bmatrix} 1 & 1/2 \\ 0 & \sqrt{3}/2 \end{bmatrix}}_{shear-compression} \tag{7}$$

Where x_t and y_t are the coordinates of the original x and y row vector element locations, when altered by transformation matrix, A. This was applied specifically to Costas arrays, though is applicable to any arrangement, and is represented pictorially in Figure 8 for a 7×7 Lempel L_2 construction, where first the array is sheared in the horizontal dimension, then compressed in the vertical dimension. Applying a spatial transformation to the element locations also applies the

same transformation to the vector separations, and hence the AACF. This means that a non-redundant square grid arrangement will, when transformed, also produce a non-redundant hexagonal one. In order to form a more isotropic array, a sequence is preferred whose elements fall close to the main diagonal, and consequently the Lempel L_2 construction is well suited. This is evident from Figure 8 where it can be seen that a 'square-footprint' array (including gray squares) would transform to a 'rhombus-footprint' array, as opposed to the hexagonal array shown (excluding gray squares). The resultant arrangement has the property of 'non-attacking bee-rooks' (from the game of hexagonal chess), whereby no two elements lie on the same line of adjacent hexagons[28]. This, like the Costas array of Figure 9d, ensures an increased minimum separation distance.

The underlying periodicity remains, though the transformation can lead to a more tightly packed yet evenly spread AACF. This is demonstrated in Figure 10 where both original square grid (a) and transformed hexagonal array (b) for a 27×27 Lempel L_2 Costas array are shown, along with their respective AACF distributions (c) and (d). These are expressed as vector separation maps where no two separations coincide. The threefold rotational symmetry of the hexagonal array is clear. The result is more consistent behavior with angle of incidence, as well as a slight improvement in scattered uniformity compared to a regular square grid due to the larger number of separation paths comparable to wavelength across the design bandwidth.

C. Amplitude Shading

In order to achieve low frequency power, cylinders of approximately a quarter wavelength in diameter are necessary. One option is to use a variety of cylinder sizes, providing elements comparable in scale to a range of wavelengths. If the scattered amplitude of each element – assumed previously to be contributing equally – could be controlled, then a sequence

of reflection coefficients may be sought where $|R_{n,m}|$ can take any positive real value. The scattered energy from a cylinder is approximately proportional to size (though demonstrating a high-pass filter shape), and so in a slightly crude manner, size can be used to vary each elements contribution. Individual element polar patterns are neglected here and are assumed to scatter omnidirectionally.

In array theory, this process is often referred to as amplitude shading, and typically involves the application of a windowing function to a full array in order to maximally suppress the sidelobes. Ideally, a sequence is required that aims to achieve equal sidelobe energy rather than restrict their level, as it is this that determines diffusive performance. An example is the Chebychev window[29] which provides a series of weightings designed to achieve a specified attenuation. Figure 11 shows a 10×10 array of cylinders (a) and f = 593Hz and 1333Hz scattered polar patterns (b) for a 2D Chebychev array designed to produce 20dB equally attenuated sidelobes. Cylinders less than 2cm in diameter have been omitted as their contribution is insignificant over this frequency range. The back-scattered polar response displays near equal lobing over a progressively larger area with increasing frequency. Above the first Bragg frequency however, notches in the diffusion coefficient become severe due to the high occupancy and hence redundancy. Furthermore, a Chebychev array still has cylinders in close proximity, and consequently does not allow cylinders larger than grid spacing ($d_e < \{d_x, d_y\}$), meaning low frequency power is insufficient.

An alternative approach is to apply amplitude shading to an existing array by multiplying with a chosen window in the spatial domain. This equates to convolution in the scattered polar domain. The objective is to smooth out the polar response by removing the more rapid fluctuations and so a window sequence shaped like a low-pass filter is desired, implying larger

objects in the centre of the array and progressively smaller objects towards the extents. Conveniently, this allows low frequency energy to penetrate into the structure and higher frequencies to scatter off the smaller outer elements. In addition, when windowed radially, a more isotropic array is formed. A suitable arrangement for amplitude shading is the hexagonal grid Lempel L_2 Costas array, as these tend to be sparsely populated towards the centre. Figure 12 shows both measured and modeled random incidence diffusion coefficient (a) and scattered power (b) for the hexagonal Costas array depicted in Figure 10b with amplitude shading. The original grid spacings were set at $d_x = d_y = 86$mm, before the transformation matrix in Eq. 7 was applied. To allow measurements to be carried out on the array, three readily available cylinder sizes (when scaled) were selected: $d_e \approx 50$mm for the outermost six, $d_e \approx 200$mm for the innermost three, and $d_e \approx 100$mm for the remaining eighteen. Random incidence values for both the diffusion coefficient and scattered power were obtained by averaging results for $\theta = 0^\circ$ to $\theta = 330^\circ$ taken in steps of 30°.

Like the optimized array, there is general good agreement between measured and modeled results, though with slight discrepancies in level at low frequency. The array demonstrates an overall reduction in severity of diffusion notches, both for random incidence and for specific angles of incidence (not shown). Performance might be improved further if these sizes were optimized.

VIII. CONCLUSIONS

A BEM model has been used to gain accurate predictions for the scattering from pseudorandom cylinder arrangements based on a periodic lattice, and this has been verified by measurements. Through considered removal or variation in size of elements informed by number

theoretic sequences, a number of design concepts have been shown to create arrays that provide suitable levels of diffusion and back-scattered power across the design bandwidth.

Sequences whose AACF properties are optimal provide the most even scattering. For fuller arrays however operational bandwidth is limited, with Bragg peaks affecting diffusion at high frequency and cylinder size limiting scattered power at low frequency. By eliminating structural similarity the detrimental effects on diffusion are minimized, producing an effectively oversampled sparse array. An example is the Costas array, which can allow cylinder size greater than lattice spacing, helping to extend the bandwidth of performance by effectively increasing the frequency of the first Bragg peak. Further improvements may be gained by transforming to a hexagonal lattice, providing more isotropic behavior due to the three-fold rotational symmetry. By applying amplitude shading, a hexagonal Costas array can be tuned to provide further improvements to diffusion as well as even back-scattered power across the design bandwidth.

Future enhancement to spatially diffusive performance might use aperiodic or randomized arrays, thus removing the restriction of periodicity entirely. This would likely rule out number theoretic designs, and optimization routines similar to the GA may be more appropriate. Alternative element shapes – perhaps pseudorandomly orientated – may also offer advantages, though it is envisaged that the lessons learnt on placement will still apply. Finally, it is hoped that the concepts presented here will be extended to a full 3D array.

ACKNOWLEDGEMENTS

This work was sponsored by the Engineering and Physical Sciences Research Council (EPSRC); EP/D031745/1.

REFERENCES

Volumetric diffusers: Pseudorandom cylinder arrays on a periodic lattice, Hughes, RJ; Angus, JAS; Cox, TJ, et al., Journal of the acoustical society of america **128(**5) 2847-2856 Published: Nov 2010, DOI 10.1121/1.3493455

[1]P. D'Antonio, and T. J. Cox, "Diffusor Application in Rooms," Appl. Acoust. **60**, 113-42 (2000).

[2]M. R. Schroeder, "Diffuse Sound Reflection by Maximum-Length Sequences," J. Acoust. Soc. Am. **57**, 149-50 (1975).

[3]M. R. Schroeder, "Binaural Dissimilarity and Optimum Ceilings for Concert Halls: More Lateral Sound Diffusion," J. Acoust. Soc. Am. **65**, 958-63 (1979).

[4]T. J. Cox, and P. D'Antonio, "Acoustic phase gratings for reduced specular reflection," Appl. Acoust. **60**, 167-86 (2000).

[5]J. A. S. Angus, and P. D'Antonio, "Two Dimensional Binary Amplitude Diffusers," *Proc. 107th Convention Audio Eng. Soc., New York, USA*, 5061 (1999).

[6]T. J. Cox, and P. D'Antonio, *Acoustic Absorbers and Diffusers: Theory, Design and Application,* 2nd Ed., London, Taylor & Francis; Ch. 9-10 (2009).

[7]H. Kuttruff, *Room Acoustics* 4th Ed., London, E. & F. N. Spon, 120 (2000).

[8]BS EN ISO 354:2003, "Acoustics - Measurement of Sound Absorption in a Reverberation Room."

[9]J. H. Rindel, "Design of New Ceiling Reflectors for Improved Ensemble in a Concert Hall," Appl. Acoust. **34**, 7-17 (1991).

[10]R. J. Hughes, J. A. S. Angus, T. J. Cox, and O. Umnova, "Volumetric Diffusers," *Proc. 124th Convention Audio Eng. Soc., Amsterdam, The Netherlands*, 7432 (2008).

[11]T. J. Cox, R. J. Hughes, J. A. S. Angus, D. M. Whittaker, M. Pogson, and G. A. Gehring, "Volume Diffusers Inspired by Percolation Fractals," *Proceedings of the Institute of Acoustics, Oslo, Norway* (2008).

Volumetric diffusers: Pseudorandom cylinder arrays on a periodic lattice, Hughes, RJ; Angus, JAS; Cox, TJ, et al., Journal of the acoustical society of america **128(**5) 2847-2856 Published: Nov 2010, DOI 10.1121/1.3493455

[12]R. J. Hughes, J. A. S. Angus, T. J. Cox, O. Umnova, D. M. Whittaker, G. A. Gehring, and M. Pogson, "Volumetric Diffusion from Pseudorandom Periodic Cylinder Arrays," *Presented at Euronoise, Edinburgh, Scotland* (2009).

[13]W. M. Robertson, and J. F. Rudy III, "Measurement of Acoustic Stop Bands in Two-Dimensional Periodic Scattering Arrays," J. Acoust. Soc. Am. **104**, 694-9 (1998).

[14]J. V. Sánchez-Pérez, D. Caballero, R. Mártinez-Sala, C. Rubio, J. Sánchez-Dehesa, F. Meseguer, J. Llinares, and F. Gálvez, "Sound Attenuation by a Two-Dimensional Array of Rigid Cylinders," Phys. Rev. Lett. **80**, 5325 (1998).

[15]T. J. Cox, "Predicting the Scattering from Reflectors and Diffusers Using Two-Dimensional Boundary Element Methods," J. Acoust. Soc. Am. **96**, 874-8 (1994).

[16]AES-4id-2001, "AES Information Document for Room Acoustics and Sound Reinforcement Systems - Characterization and Measurement of Surface Scattering Uniformity," J. Audio Eng. Soc. **49**, 149-65 (2001).

[17]J.-J. Rousseau, *Basic Crystallography*, Chichester; New York NY, John Wiley & Sons, 148 (c1998).

[18]G. S. Bloom, and S. W. Golomb, "Applications of Numbered Undirected Graphs," Proc. IEEE **65**, 562-70 (1977).

[19]J. A. S. Angus, "Using Grating Modulation to Achieve Wideband Large Area Diffusers," Appl. Acoust. **60**, 143-65 (2000).

[20]E. Vertatschitsch, and S. Haykin, "Nonredundant Arrays," Proc. IEEE **74**, 217 (1986).

[21]M. R. Schroeder, *Number Theory in Science and Communication : With Applications in Cryptography, Physics, Digital Information, Computing, and Self-Similarity*, 3rd Ed., Springer series in information sciences: No. 7, Berlin; London, Springer, 190 (1997).

Volumetric diffusers: Pseudorandom cylinder arrays on a periodic lattice, Hughes, RJ; Angus, JAS; Cox, TJ, et al., Journal of the acoustical society of america **128(**5) 2847-2856 Published: Nov 2010, DOI 10.1121/1.3493455

[22]Y. Meurisse, and J.-P. Delmas, "Bounds for Sparse Planar and Volume Arrays," IEEE Trans. Inf.Theory **47**, 464-8 (2001).

[23]V. Romero-Garcia, E. Fuster, L. M. Garcia-Raffi, E. A. Sanchez-Perez, M. Sopena, J. Llinares, and J. V. Sanchez-Perez, "Band Gap Creation Using Quasiordered Structures Based on Sonic Crystals," Appl. Phys. Lett. **88** (2006).

[24]A. Hakansson, F. Cervera, and J. Sanchez-Dehesa, "Sound Focusing by Flat Acoustic Lenses Without Negative Refraction," Appl. Phys. Lett. **86**, 054102 (2005).

[25]T. J. Cox, B.-I. L. Dalenback, P. D'Antonio, J. J. Embrechts, J. Y. Jeon, E. Mommertz, and M. Vorländer, "A Tutorial on Scattering and Diffusion Coefficients for Room Acoustic Surfaces," Acta Acust. United Ac. **92**, 1-15 (2006).

[26]P. Robinson, and N. Xiang, "On the Subtraction Method for In-Situ Reflection and Diffusion Coefficient Measurements," J. Acoust. Soc. Am. **127**, EL99-EL104 (2010).

[27]C. Hammond, *The Basics of Crystallography and Diffraction*, International Union of Crystallography texts on crystallography: No. 3, Oxford, Oxford University Press, 163 (1997).

[28]S. W. Golomb, and H. Taylor, "Constructions and Properties of Costas Arrays," Proc. IEEE **72**, 1143-63 (1984).

[29]H. L. Van Trees, *Optimum Array Processing: Part IV of Detection, Estimation and Modulation Theory*, New York NY; Chichester, Wiley-Interscience, 264-267 (2002).

FIGURE CAPTIONS

Figure 1: Arrangement (a) and semi-anechoic measurement setup (b) for a 10×10 Cylinder array with 25% occupancy optimized using a Genetic Algorithm and a 2D Fourier approximation.

Volumetric diffusers: Pseudorandom cylinder arrays on a periodic lattice, Hughes, RJ; Angus, JAS; Cox, TJ, et al., Journal of the acoustical society of america **128(**5) 2847-2856 Published: Nov 2010, DOI 10.1121/1.3493455

Figure 2: The scattered field around a 2D volume diffuser. Definition of the Back-Scattered Zone (BSZ); Forward Scattered Zone (FSZ); Geometric Visible Zone (GVZ); and Geometric Shadow Zone (GSZ) around a cylinder array of width D.

Figure 3: Far field single scattering p_s at receiver angle θ_r, from an $M \times N$ periodically spaced rectangular grid of point scatterers with unit spacing d_x and d_y in the x and y directions respectively, subject to a plane wave p_i, incident from angle θ.

Figure 4: BAD panel (a) and cylinders (b) arranged according to an $N = 7$ (perfect) Golomb ruler.

Figure 5: Diffusion coefficient (a) and AACF (b) for MLS cylinder sequences [1 1 0 0 1 0 1] and [0 0 1 0 1 1 1], d_y = 200mm, d_e = 100mm.

Figure 6: Measured and modeled scattered field for a 10×10 array (as per Figure 1), f = 1050Hz (a) and 1600Hz (b).

Figure 7: Diffusion coefficient (a), and back-scattered power (b), including predicted Bragg frequencies, $f_{\alpha,\beta}$, for the 10×10 array (as per Figure 1).

Figure 8: Transformation of a 7×7 Lempel L2 Costas array from a square lattice to a hexagonal lattice via shearing and then compression (shear-compression) – after Golomb *et al*.[28].

Figure 9: Diffusion coefficient (a), back-scattered power (b), and AACF (c), for a 15×15 T_4 Costas array of cylinders (d).

Figure 10: Square grid (a) and transformed hexagonal array (b) for a 27×27 Lempel L_2 Costas construction, along with respective AACF vector spacings (c) and (d).

Figure 11: Arrangement (a) and scattered pressure at f = 593Hz and 1333Hz (b) for a 10×10 amplitude shaded array determined by a 2D Chebychev sequence.

Volumetric diffusers: Pseudorandom cylinder arrays on a periodic lattice, Hughes, RJ; Angus, JAS; Cox, TJ, et al., Journal of the acoustical society of america **128(**5) 2847-2856 Published: Nov 2010, DOI 10.1121/1.3493455

Figure 12: Measured and modeled random incidence diffusion coefficient (a) and back-scattered power (b) for a 27×27 amplitude shaded Lempel L_2 Costas hexagonal grid array.

Volumetric diffusers: Pseudorandom cylinder arrays on a periodic lattice, Hughes, RJ; Angus, JAS; Cox, TJ, et al., Journal of the acoustical society of america **128(**5) 2847-2856 Published: Nov 2010, DOI 10.1121/1.3493455

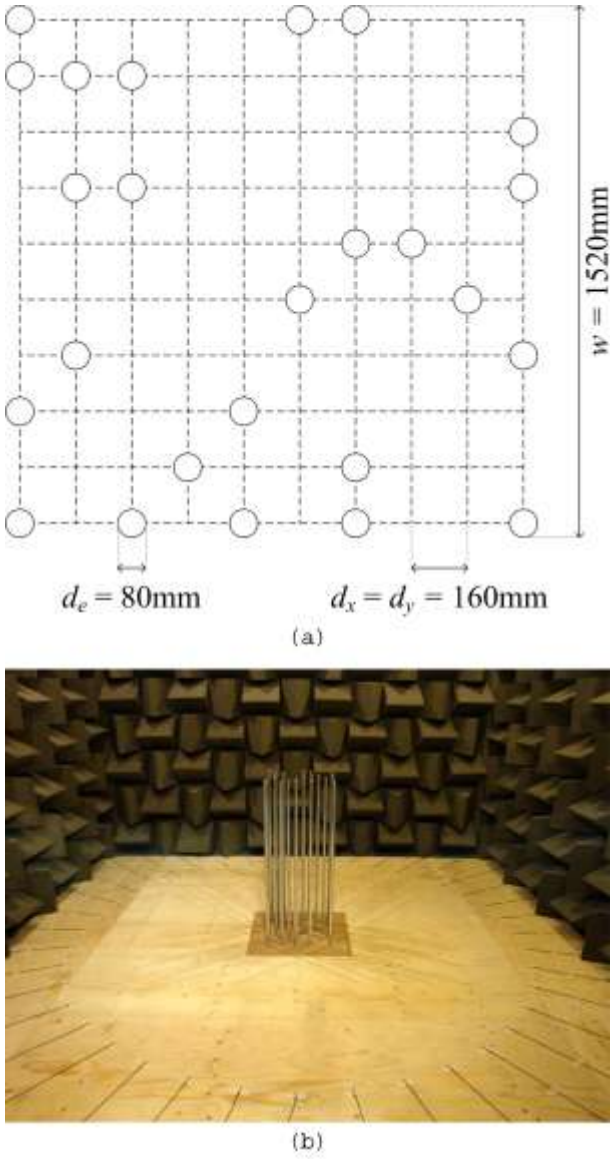

Figure 1

Volumetric diffusers: Pseudorandom cylinder arrays on a periodic lattice, Hughes, RJ; Angus, JAS; Cox, TJ, et al., Journal of the acoustical society of america **128(**5) 2847-2856 Published: Nov 2010, DOI 10.1121/1.3493455

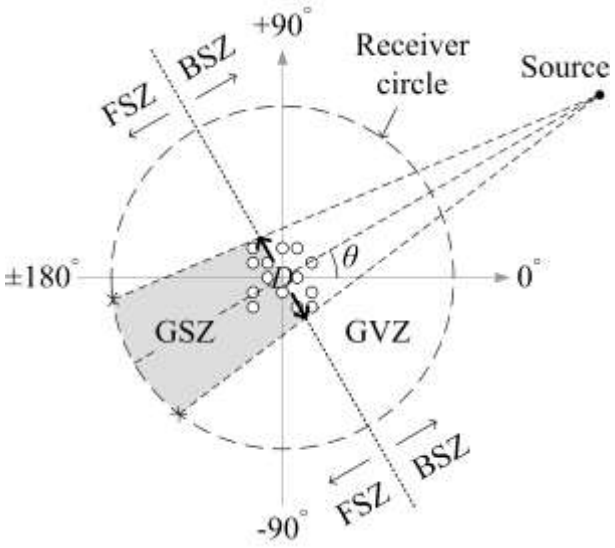

Figure 2

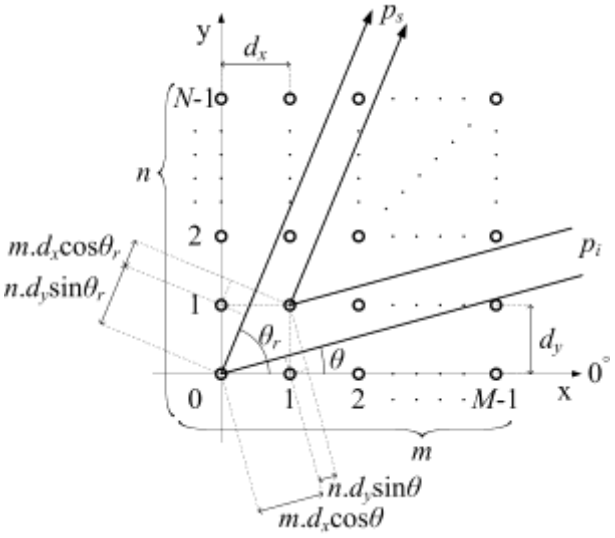

Figure 3

Volumetric diffusers: Pseudorandom cylinder arrays on a periodic lattice, Hughes, RJ; Angus, JAS; Cox, TJ, et al., Journal of the acoustical society of america **128(**5) 2847-2856 Published: Nov 2010, DOI 10.1121/1.3493455

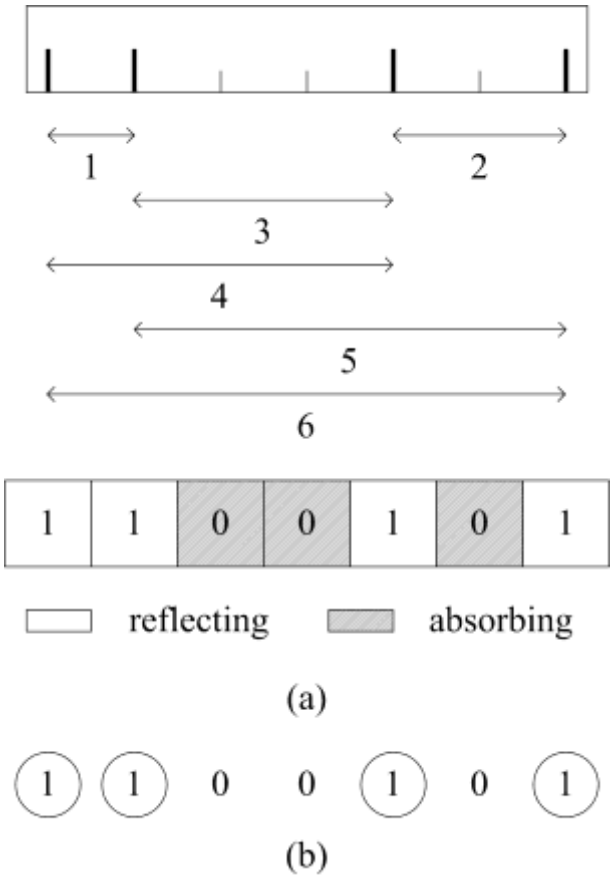

Figure 4

Volumetric diffusers: Pseudorandom cylinder arrays on a periodic lattice, Hughes, RJ; Angus, JAS; Cox, TJ, et al., Journal of the acoustical society of america **128(**5) 2847-2856 Published: Nov 2010, DOI 10.1121/1.3493455

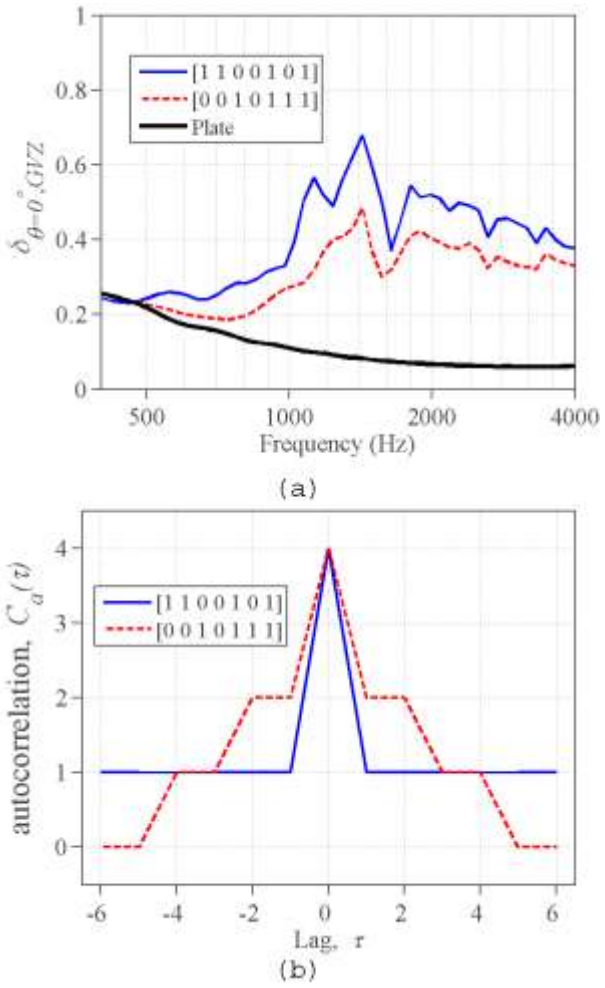

Figure 5

Volumetric diffusers: Pseudorandom cylinder arrays on a periodic lattice, Hughes, RJ; Angus, JAS; Cox, TJ, et al., Journal of the acoustical society of america **128(**5) 2847-2856 Published: Nov 2010, DOI 10.1121/1.3493455

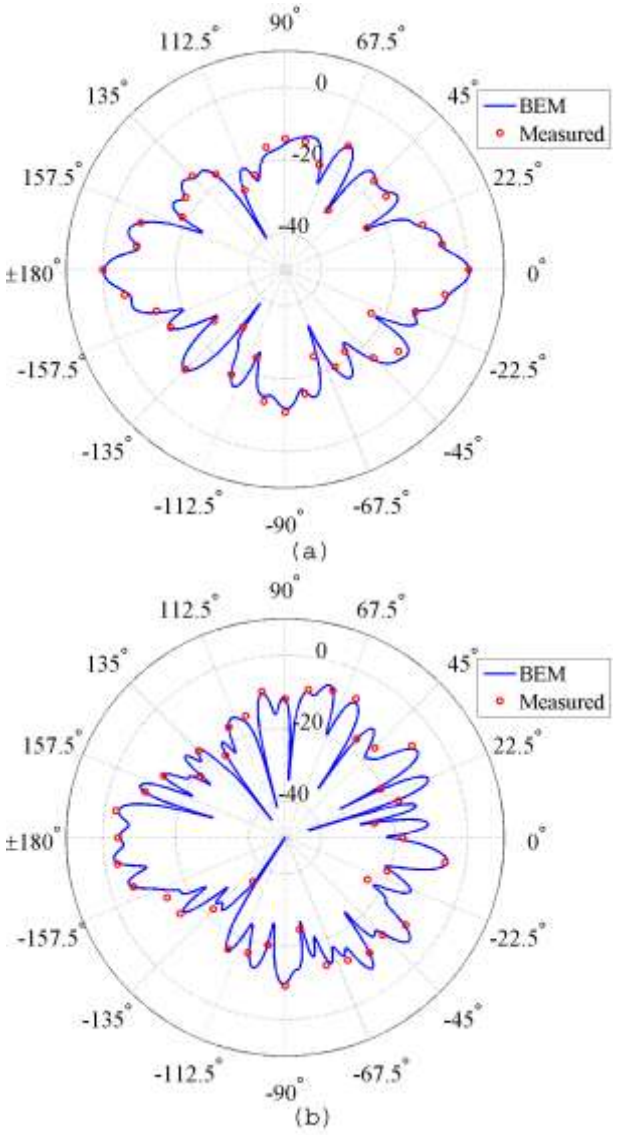

Figure 6

Volumetric diffusers: Pseudorandom cylinder arrays on a periodic lattice, Hughes, RJ; Angus, JAS; Cox, TJ, et al., Journal of the acoustical society of america **128(**5) 2847-2856 Published: Nov 2010, DOI 10.1121/1.3493455

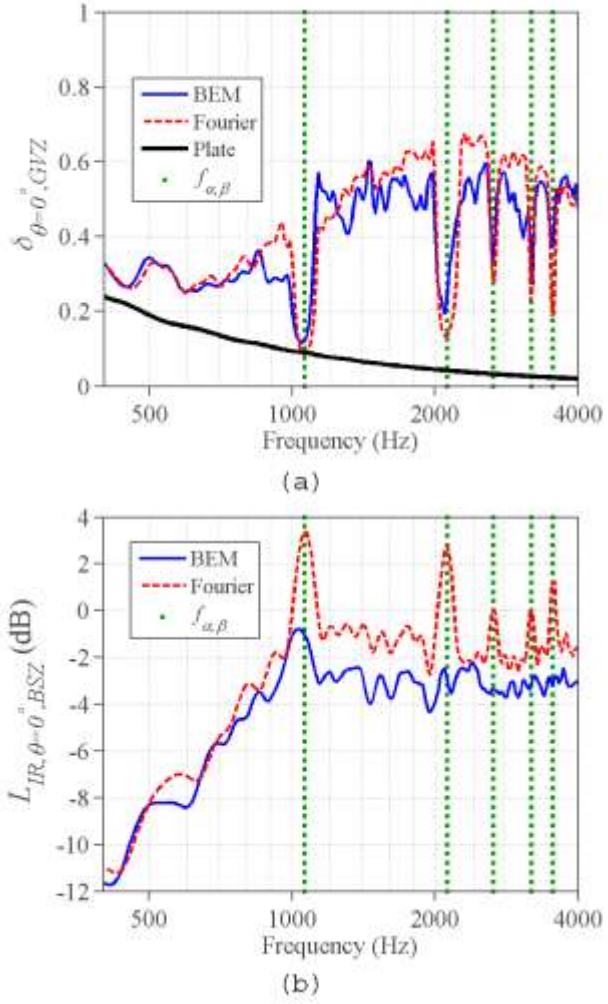

Figure 7

Volumetric diffusers: Pseudorandom cylinder arrays on a periodic lattice, Hughes, RJ; Angus, JAS; Cox, TJ, et al., Journal of the acoustical society of america **128(**5) 2847-2856 Published: Nov 2010, DOI 10.1121/1.3493455

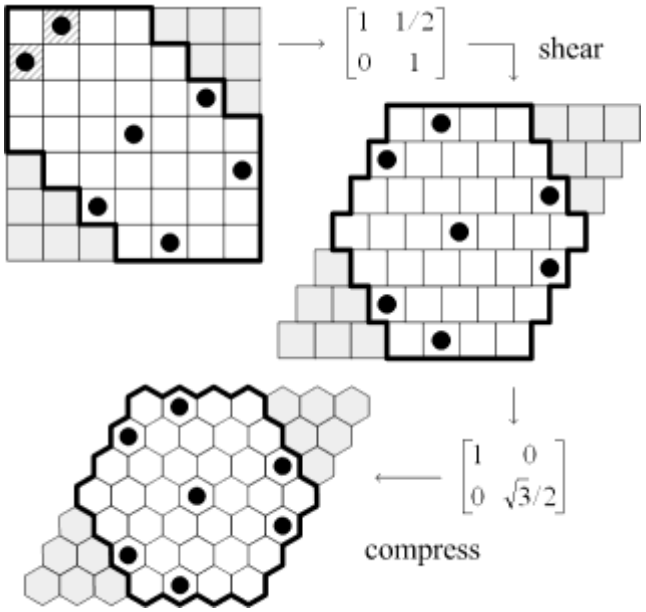

Figure 8

Volumetric diffusers: Pseudorandom cylinder arrays on a periodic lattice, Hughes, RJ; Angus, JAS; Cox, TJ, et al., Journal of the acoustical society of america **128(**5) 2847-2856 Published: Nov 2010, DOI 10.1121/1.3493455

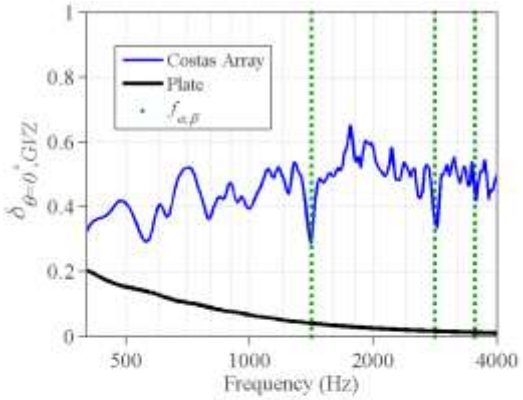

(a)

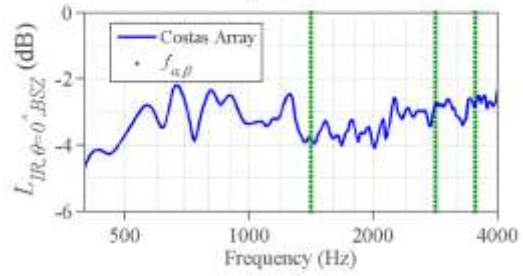

(b)

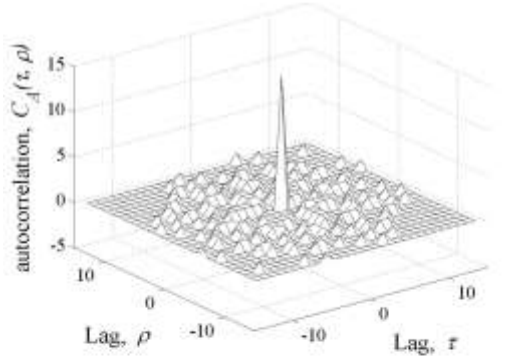

(c)

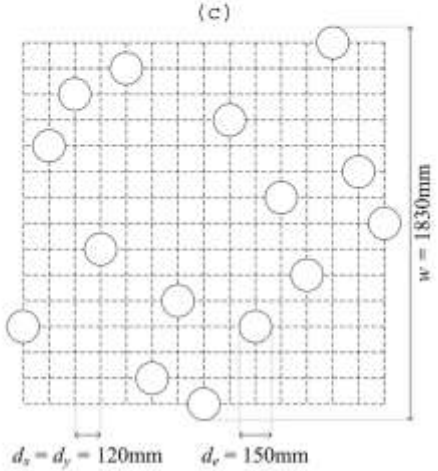

(d)

Volumetric diffusers: Pseudorandom cylinder arrays on a periodic lattice, Hughes, RJ; Angus, JAS; Cox, TJ, et al., Journal of the acoustical society of america **128(**5) 2847-2856 Published: Nov 2010, DOI 10.1121/1.3493455

Figure 9

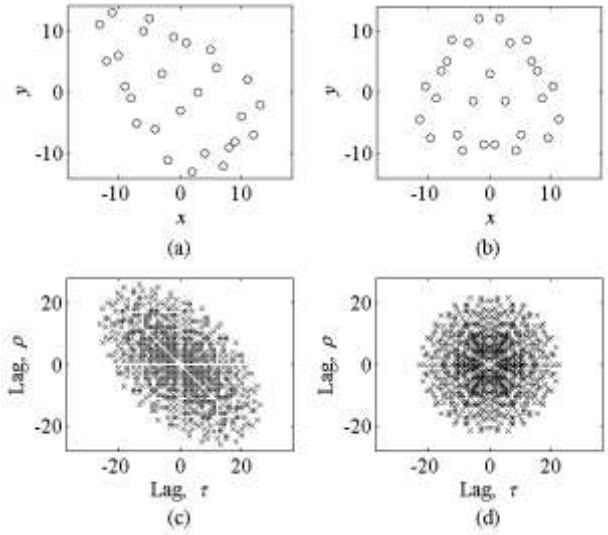

Figure 10

Volumetric diffusers: Pseudorandom cylinder arrays on a periodic lattice, Hughes, RJ; Angus, JAS; Cox, TJ, et al., Journal of the acoustical society of america **128(**5) 2847-2856 Published: Nov 2010, DOI 10.1121/1.3493455

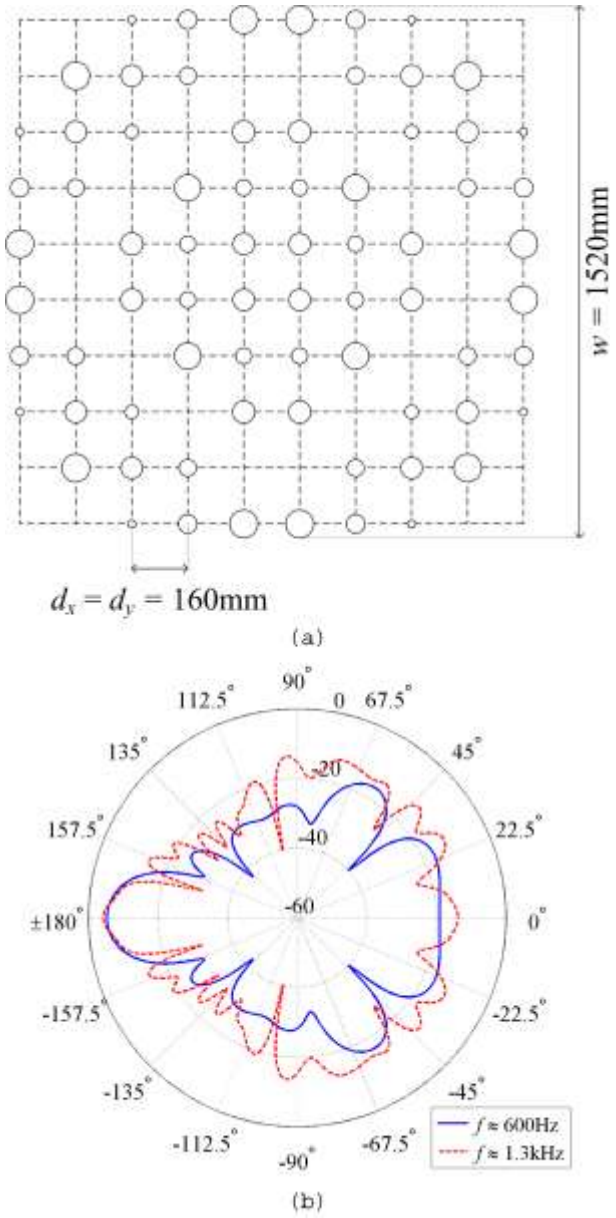

Figure 11

Volumetric diffusers: Pseudorandom cylinder arrays on a periodic lattice, Hughes, RJ; Angus, JAS; Cox, TJ, et al., Journal of the acoustical society of america **128(**5) 2847-2856 Published: Nov 2010, DOI 10.1121/1.3493455

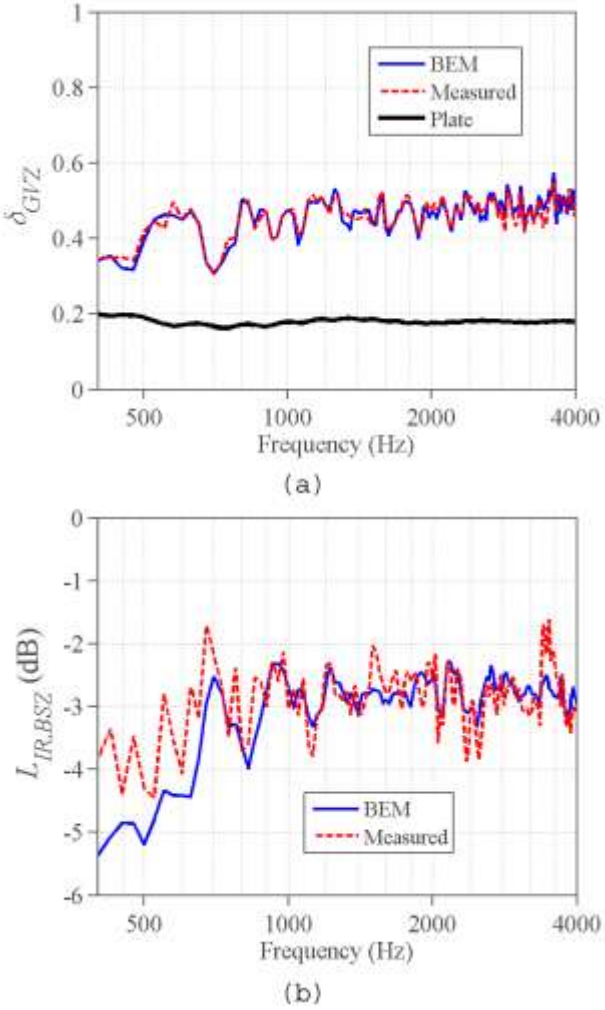

Figure 12